

TIDAL STIRRING AND THE ORIGIN OF DWARF SPHEROIDALS IN THE LOCAL GROUP

LUCIO MAYER^{1,4}, FABIO GOVERNATO², MONICA COLPI¹, BEN MOORE³, THOMAS QUINN⁴, JAMES WADSLEY^{4,5}, JOACHIM STADEL⁴ & GEORGE LAKE⁴¹Dipartimento di Fisica, Università Degli Studi di Milano Bicocca, via Celoria 16, I-20133 Milano, Italy²Osservatorio Astronomico di Brera, via Bianchi 46, I-23807 Merate (LC) - Italy³Department of Astronomy, University of Durham, Durham, U.K, DH1 3LE⁴Department of Astronomy, University of Washington Seattle, USA, WA 98196⁵Department of Physics and Astronomy, McMaster University, Hamilton, Ontario L8S 4M1 Canada*To appear in ApJL*

ABSTRACT

N-body + SPH simulations are used to study the evolution of dwarf irregular galaxies (dIrrs) entering the dark matter halo of the Milky Way or M31 on plunging orbits. We propose a new dynamical mechanism driving the evolution of gas rich, rotationally supported dIrrs, mostly found at the outskirts of the Local Group (LG), into gas free, pressure supported dwarf spheroidals (dSphs) or dwarf ellipticals (dEs), observed to cluster around the two giant spirals. The initial model galaxies are exponential disks embedded in massive dark matter halos and reproduce nearby dIrrs. Repeated tidal shocks at the pericenter of their orbit partially strip their halo and disk and trigger dynamical instabilities that dramatically reshape their stellar component. After only 2-3 orbits low surface brightness (LSB) dIrrs are transformed into dSphs, while high surface brightness (HSB) dIrrs evolve into dEs. This evolutionary mechanism naturally leads to the morphology-density relation observed for LG dwarfs. Dwarfs surrounded by very dense dark matter halos, like the archetypical dIrr GR8, are turned into Draco or Ursa Minor, the faintest and most dark matter dominated among LG dSphs. If disks include a gaseous component, this is both tidally stripped and consumed in periodic bursts of star formation. The resulting star formation histories are in good qualitative agreement with those derived using HST color-magnitude diagrams for local dSphs.

Subject headings: galaxies: Local Group — galaxies: dwarfs — galaxies: evolution — galaxies: kinematics and dynamics — galaxies: interactions — methods: N-Body simulations

1. INTRODUCTION

Dwarf galaxies in the Local Group (LG) clearly obey a morphology-density relation. Close to the Milky Way and M31 we find early-type dwarf galaxies, namely faint ($M_B > -14$) low surface brightness dwarf spheroidals (dSphs) and more luminous ($M_B > -17$), higher surface brightness dwarf ellipticals (dEs). All these galaxies are nearly devoid of gas, contain dark matter and mainly old stars and are supported by velocity dispersion (Ferguson & Bingeli 1994, hereafter FB94; Mateo 1998, hereafter Ma98; Grebel 1999, hereafter Gr99; Van den Bergh 1999). Among them Draco and Ursa Minor have the highest dark matter densities ever measured (Lake 1990). On the outskirts of the LG we find similarly faint ($M_B > -18$) and dark matter dominated dwarf irregular galaxies (dIrrs), that are gas rich, star-forming systems with disk-like kinematics (Ma98, Van den Bergh 1999, Gr99).

Previous attempts to explain the origin of dSphs in the LG have relied on gas dynamical processes to remove the gas in dIrrs. Gas stripping may result either because of the pressure exerted by an external hot gaseous medium in the halo of the Milky Way (“ram pressure”) (Einasto et al. 1974) or because of internal strong supernovae winds (Dekel & Silk 1986). However, ram pressure would require an external gas density that is several orders of magnitude higher than recently inferred for the Milky Way (Murali 2000) and supernovae winds cannot explain the existing morphology-density relation. Moreover, such dissipative mechanisms would remove the gas but would not directly

alter the structure and kinematics of the pre-existing stellar component. However, the light follows an exponential profile in both dSphs and dIrrs (Faber & Lin 1983; Irwin & Hatzidimitriou 1995; Ma98) and a positive correlation between surface brightness and luminosity is shown by both types of dwarfs (FB94), suggesting an evolutionary link between them. Is there a mechanism that can transform dwarf galaxies between morphological classes or must we accept the idea that dSphs are fundamentally different from dIrrs ?

Within rich galaxy clusters, fast fly-by encounters with the largest galaxies can transform a disk system into a spheroidal or S0 galaxy in just 3-4 Gyr (Moore et al. 1996, 1998). If the halos of bright galaxies were scaled down versions of galaxy clusters then this “galaxy harassment” would be equally important within them. However, whereas rich clusters contain over thirty large (L_*) perturbing galaxies, the Milky Way and M31 have only a couple of satellites sufficiently massive to harass the other dwarf galaxies (Moore et al. 1999; Klypin et al. 1999). As a result, the rate for effective satellite-satellite fly-by encounters is less than one in every 10 Gyr (the LMC and the SMC being a notable exception).

Thus, we are left only with the repeated action of tidal forces from the primary galaxy as an evolutionary driver. These operate on the orbital timescale, which is of order of 3-4 Gyr in both clusters and galactic halos. However, given the relatively low age of large, virialized clusters, galaxies have typically approached the cluster center only

once by the present time, while dSphs satellites have had sufficient time to complete several close tidal encounters with the Milky Way, as stellar ages imply that the latter was already in place 10 Gyr ago (Van den Bergh 1996).

In this paper we use very high resolution N-Body + SPH simulations performed with the parallel binary treecode GASOLINE (Dikaiakos & Stadel 1996; Wadsley et al. 2000) to follow the evolution of small galaxies resembling dIrrs as they move on bound orbits in the tidal field of the massive dark matter halo of the Milky Way.

2. MODELS OF DWARF GALAXIES

The Milky Way halo is modeled as the fixed potential of a truncated isothermal sphere with a total mass $4 \times 10^{12} M_{\odot}$ inside a radius of 400 kpc, consistent with both recent measures based on radial velocities of distant satellites (Wilkinson & Evans 1999) and with generic models of structure formation (Peebles et al. 1989). The core radius is 4 kpc and the resulting circular velocity at the solar radius is 220 km/s.

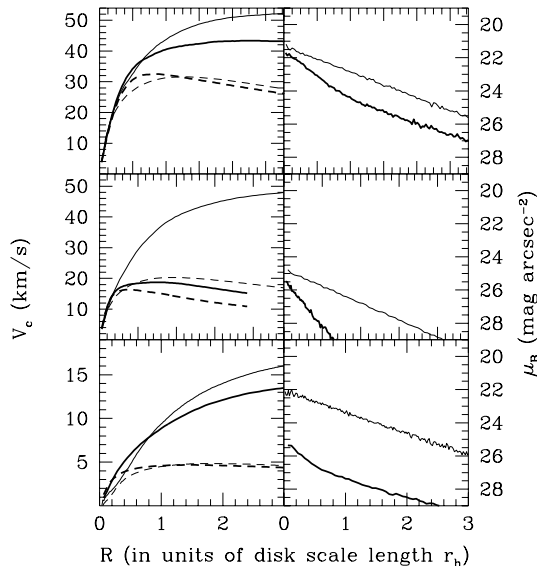


Fig. 1.— Evolution of circular velocity (left) and surface brightness profiles (right) for our model galaxies: thin lines are used for the initial profiles, thick lines for the profiles after 7 Gyr. From top to bottom, models *M2H*, *M2La* and *GR8* are shown. The overall (stars + dark matter) circular velocity profile is always represented by a solid line, while a dashed line describes the contribution of the stellar component alone. For the final surface brightness profile we take into account fading according to the star formation history described in the text. We assume that the last burst occurs 4 Gyr ago for HSBs and LSBs and 7 Gyr ago for GR8, thus resulting in a more pronounced fading for the latter. The different choices correspond to the different epochs of infall inferred from our evolutionary model. The orbits had an apo/peri of 9 and a pericenter of ~ 40 kpc (HSBs and LSBs) and 12 kpc (GR8), with random disk orientations.

Our simulated galaxies are modeled as exponential disks of stars with a Toomre parameter $Q = 2$ embedded in truncated isothermal dark matter halos (see Hernquist 1993). The number of particles in the disk is 50,000 while that in

the halo ranges from 250,000 to 3×10^6 . Such high resolution in the halo reduces considerably numerical heating of the disk due to massive halo particles, as was tested by evolving our models in isolation for 5 Gyr. The scale-lengths and masses of the stellar disk and dark matter halo are chosen so that the satellites follow the observed B band Tully-Fisher relation (Hoffman et al. 1996; Zwaan et al. 1997) and have realistic rotation curves (de Blok & McGaugh 1997; Cote et al. 1997), as shown in Figure 1. The determination of general scaling properties of galaxies becomes more uncertain at the very faint end. Current structure formation models predict that the mass M and scale radius R of halos (and of their embedded disks) vary with redshift as $\sim (1+z)^{-3/2}$ for a fixed value of the circular velocity V_c , with $V_c \sim R \sim M^{1/3}$ (Mo et al. 1998).

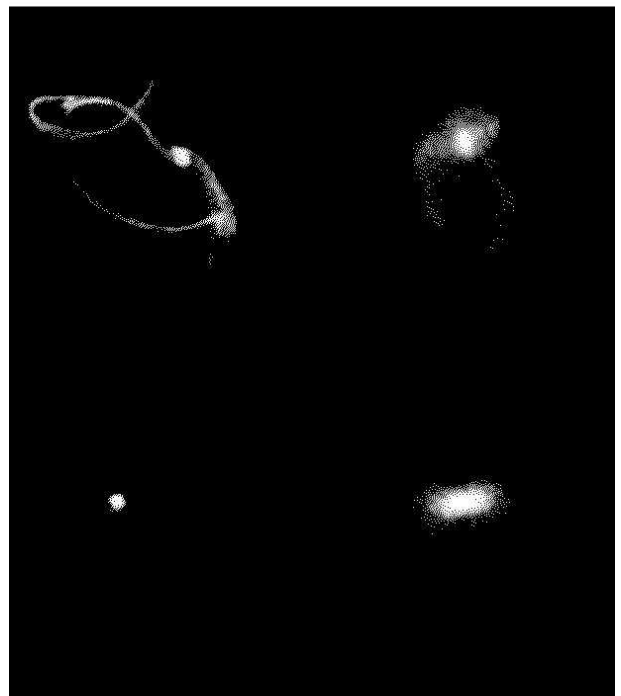


Fig. 2.— The final stellar configurations of our model galaxies. Left panels show the stellar streams of the LSB (upper) and HSB (lower) satellites viewed face on (the orbit has apo/peri=4). The boxes are 500 kpc on a side, with brighter colors showing regions with higher density. Right panels show close up views of the remnants seen edge-on in frames of 50 kpc on a side.

The scaling with redshift reflects the fact that low mass halos form at early epochs and have higher characteristic densities because the average density of the Universe was higher. Galaxies with total masses $< 10^9 M_{\odot}$ should typically form at $z \geq 2$ (Lacey & Cole 1993) and should live in halos with a central dark matter density $\sim 0.3 M_{\odot} \text{pc}^{-3}$, comparable to what inferred for GR8, an extremely faint LG dIrr (Carignan et al. 1990). The model with the smallest mass (“GR8”) was built following these prescriptions.

The models cover the entire luminosity function of irregulars in the LG (Ma98) with stellar masses of $1.2 \times 10^6 M_{\odot}$ ($M_B = -11.2$, “GR8”), $9 \times 10^8 M_{\odot}$ ($M_B = -16.23$, “M2”))

and 2.5×10^9 ($M_B = -18$, “M1”). At fixed disk mass (either M1 or M2) we also vary the disk scale length, obtaining high surface brightness (HSBs, $\mu_B = 21.5$ mag arcsec $^{-2}$, M1H and M2H) or low surface brightness satellites (LSBs, $\mu_B = 24.5$ or 23.5 mag arcsec $^{-2}$, M1La, M2La, M2Lb) for a total of six different models (we always assume $M/L_B = 2$ for the stellar disk and set the halo core radius equal to the disk scale length; see de Blok & McGaugh 1997). The GR8 model was obtained by rescaling model M1La for $z = 2$. The disk scale-length r_h is only 76 pc for GR8, while those of the other models are, respectively, 1.3 or 2 kpc (HSBs) and 1.5, 3.2 or 4.8 kpc (LSBs). The total mass-to-light ratios at $3r_h$ (close to the peak of the rotation curves) are, respectively, 6 (HSBs), 12 (LSBs) and 32 (GR8).

3. EVOLUTION OF DWARF GALAXIES

As the Milky Way halo is modeled as an external potential, dynamical friction is neglected, which is a good approximation for satellites ~ 100 times less massive than the primary halo (Colpi et al. 1999). Satellites start at the virial radius of the primary (their apocenter) as if they were infalling for the first time, moving on orbits whose ratio between apocenter and pericenter ranges from 4 to 10, in agreement with simulations of galaxy and cluster formation (Ghigna 1998). Orbital periods are typically of the order of 3 – 4 Gyr, but are as short as 1 – 2 Gyr in the run with GR8, because this model was evolved in a Milky Way potential scaled down in size and mass as expected at $z = 2$. The inclination and spin of the disk relative to the orbital plane are randomly selected. In total 40 different runs were performed.

3.1. Dynamical Evolution

As the dwarfs approach pericenter (typically of 40-70 kpc) LSBs lose most of their dark matter halo and stars, due to their low density halos and large disks, and become weakly bar unstable. HSBs suffer modest stripping and their more self-gravitating disks develop a strong bar. The GR8 model is barely stripped owing to its very dense halo and its small disk radius. Minimal stripping keeps its disk more self gravitating compared to the structurally similar LSB and thus a fairly strong bar can develop after the second pericenter passage. Mass stripping for the various models is reflected in the evolution of their circular velocity profiles (Figure 1).

After completion of 2-3 orbits in 7 Gyr, our “tidally stirred” dwarf galaxies bear a striking resemblance to the real dSphs (right panel in Figure 2): direct tidal heating coupled with the buckling of the bar due to bending instabilities (Raha et al. 1991) transmute the small disks into spheroids supported by velocity dispersion instead of rotation (Figure 3). The GR8-like dwarf, falling into the Milky Way halo around redshift 2, suffers several (5) strong tidal shocks by the present time and is thus transformed despite being extremely compact.

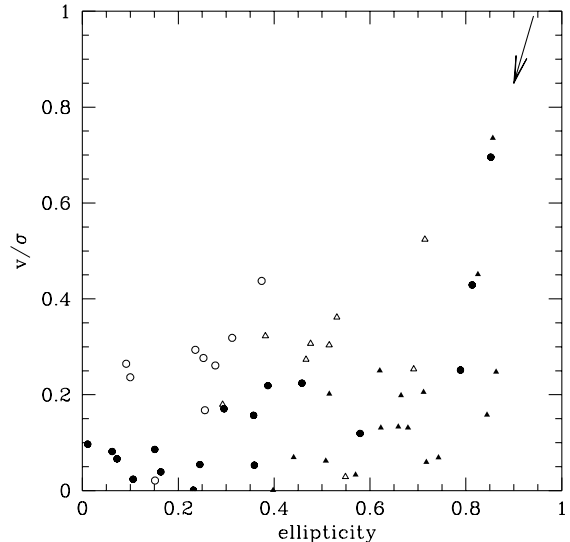


Fig. 3.— The final v/σ normalized to the initial value is plotted against the final ellipticity for 26 different runs. For each final state we show the measurements for a line-of-sight aligned with the major axis of the remnant (circles) and with the intermediate axis of the remnant (triangles). Minor axis projections are not shown because rotation along the other two axes is negligible. Filled symbols are for LSBs, open symbols are for HSBs. The arrow starts at the coordinates of the initial states of all the satellites and shows the direction of evolution. The ellipticity is either $1 - c/b$ or $1 - c/a$ (with a, b and c being, respectively, the major, intermediate and minor axis of the remnants) depending on the projection.

On average the final v/σ (i.e. the ratio of the rotational to random velocity) inside the half mass radius R_e drops mean values ≤ 0.5 and σ varies in the range 7 – 35 km s $^{-1}$, as observed for dSphs and dEs in the LG (Ma98). The largest of these values are typical of HSB remnants and are comparable to the velocity dispersion measured for the dEs associated to M31 (Ma98; Kormendy 1987). Only when the satellite is initially in retrograde rotation with respect to its orbital motion we measure a final v/σ still close to 1. The surface brightness profiles remain close to exponential (Figure 1), although with a smaller scale-length (typically by a factor of ~ 2). The remnants of HSBs exhibit a more pronounced steepening of the profile inside R_e because stars more efficiently lose angular momentum due to the strong bar instability. A From this set of more than 40 runs a clear trend emerges: *LSBs evolve into objects resembling dSphs while HSBs transmute into dEs.*

3.2. Gasdynamics and star formation history

Dwarf irregular galaxies have in general extended gaseous disks with an average total HI-to-stellar mass ratio larger than one (Hoffman et al. 1996): however, within the optical radius ($\sim 3 r_h$), the neutral hydrogen fraction often drops to only 50% of the stellar mass (Jobin & Carignan 1990; Cote et al. 1990). In some of our model galaxies we include a gaseous disk of 20,000 particles which only extends out to the radius of the stellar disk (material lying outside this radius is entirely stripped according to the col-

lisionless runs) and whose mass is 30% of the total baryonic mass (the gas density drops to zero at a radius $R < 0.5r_h$ to mimic the “holes” found in many dIrrs). The dynamics of gas are implemented using an SPH scheme and radiative cooling for a primordial mixture of hydrogen and helium (Wadsley et al. 2000). The initial temperature of the gas is set at 5000 K.

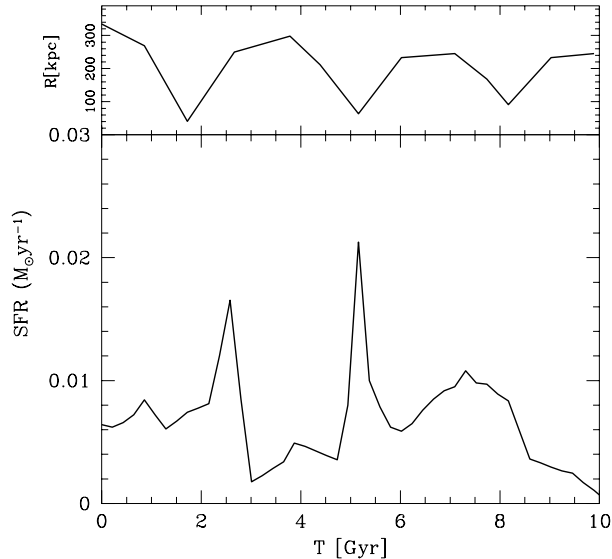


Fig. 4.— Star formation history for an LSB dwarf. We assume that the dwarf enters the Milky Way halo 10 Gyr ago ($t=0$ is the present time). The evolution of the radial orbital oscillation is also shown in the small panel on top.

We place an LSB satellite (model M2La) on a 9:1 orbit: $\sim 50\%$ of the gas is stripped after two pericenter passages and is never reaccreted, while the rest is torqued by the weak bar and gradually flows to the center: the surface density profile of the gas bound to the system steepens remarkably at each pericenter passage due to tidal compression and torques. We then use the Kennicutt’s law (Kennicutt 1998) to determine the star formation rate from the gas surface density. We also take into account the reduction of the gas mass as it is converted into stars. The resulting star formation history has two main peaks roughly separated by the orbital time of the dwarf (~ 3.5 Gyr) (Figure 4), as recently found for Leo I and Carina (Hernandez et al. 2000). After 10 Gyr the star formation is suppressed because of gas consumption. The stronger bar instability in an HSB (model M2H) placed on the same orbit funnels more than 80% of the gas to the center at the first pericentric passage, giving rise to a starburst ten times stronger than the bursts in the LSB and using up all the gas in ~ 2 Gyr. As the strength of the bar instability seems to determine the type of star formation history, including gas in the GR8 model would lead to a result qualitatively similar to that of the HSB. Interestingly, in the LG both the dEs and the extreme dSphs like Draco and Ursa Minor formed the bulk of their stellar population during a single early episode (Ma98: Gr99).

Finally we convolve the star formation history with the passive luminosity evolution of the stellar component resulting from population synthesis models (Bruzual & Charlot 1993) for low-metallicity systems (1/4 of the so-

lar value). The multiple bursts are modeled as decreasing exponential laws with amplitude and time constants constrained by the numerical results. The resulting total B band luminosities and stellar mass-to-light ratios of the final remnants are in good agreement with those of observed dSphs.

4. DISCUSSION

Figure 5 summarizes the main observable properties of the simulated satellites projecting them on the Fundamental Plane (FB94). The remnants of LSB satellites resemble dSphs like Fornax or Sagittarius ($-14 < M_B < -11$), while HSBs transform in the bright dEs ($M_B > -17$), having a final central surface brightness higher than that of observed dIrrs with the same luminosities and therefore matching another observational constraint (FB94;Ma98). The total (including dark matter) final mass-to-light ratios are in the range 6 – 20. Remarkably, our model can reproduce the properties of even the most extreme dSphs, Draco and Ursa Minor. In fact, as the dark matter halo of GR8 is barely affected by tides (Figure 1), the remnant ($M_B = -7.5$) has a final mass-to-light ratio still ~ 50 and the central dark matter density is still around $0.3M_\odot \text{pc}^{-3}$, matching the structural parameters inferred for Draco and Ursa Minor (Ma98).

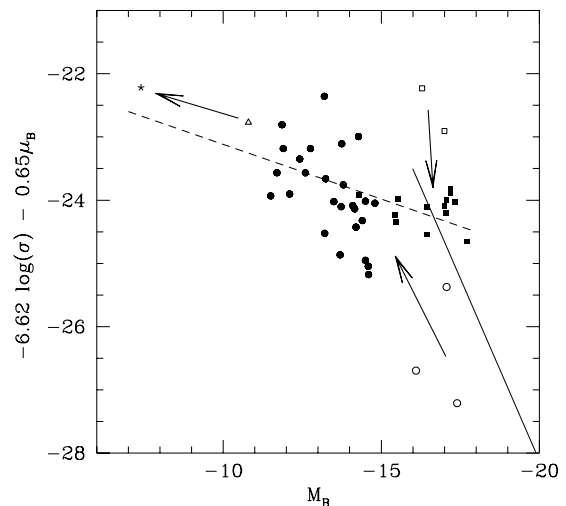


Fig. 5.— Fundamental Plane (FP) for all the remnants as in Ferguson & Binggeli (1994) (bottom). In the FP plot, μ and σ are, respectively, the average surface brightness and velocity dispersion measured inside R_e and M_B is measured at the Holmberg radius. The dashed line is a fit to the distribution of local dSphs, while the solid line refers to elliptical galaxies within the Virgo cluster (Dressler et al. 1987). Open and filled symbols represent, respectively, the initial and final state of HSBs (squares) and LSBs (circles). The initial and final state of the GR8 model are indicated by the open triangle and “star”.

“Tidal stirring” naturally leads to the spatial segregation of dIrrs versus dSph as its effectiveness depends strongly on the distance from the primary. How important is our assumption of a massive and extended dark

matter halo surrounding the Milky Way ? When we adopt a “minimal” dark halo truncated at 50 kpc (with mass $5 \times 10^{11} M_{\odot}$; Little & Tremaine 1987), tides are too weak and the final remnants are still rotationally flattened ($v/\sigma > 1$). Instead, within a halo as massive and extended as implied by theories of galaxy formation (Peebles 1989), our dIrrs models transform into dSphs even on orbits with apocenters larger than 200 kpc, explaining the origin of even the farthest dSphs as Leo I and Leo II.

Though rather speculative at this stage, it is tempting to relate HSB satellites observed during the strong bursting phase to the population of blue compact dwarfs identified by Guzmán et al. (1997) at intermediate redshift. Redshift surveys will establish if bursting dwarfs have nearby massive companions.

Extended tidal streams of stars originate from our simulated dwarfs (Fig. 2) with a maximum surface brightness

of just 30 mag arcsec⁻² (B band). Spectroscopic evidence for stellar streams from the dSph Carina has been recently claimed (Majewski et al. 2000). Future astrometric missions, like SIM and GAIA (Gilmore et al. 1998; Helmi et al. 2000) should reveal such faint features and will also carry out high-quality measurements of proper motions for many satellites of the Milky Way, thus providing a test for the orbital configurations used in this model.

Our model successfully explains the origin of dSphs once all observational constraints are taken into account: they evolved from dIrrs that entered the halo of the Milky Way or M31 several Gyr ago moving on plunging orbits and suffered stirring by the tidal field of the large spirals.

The authors thank G.Bothun for stimulating discussions. Simulations were carried out at the CINECA (Bologna) and ARSC (Fairbanks) supercomputing centers.

REFERENCES

- Bruzual G., & Charlot S. 1993, ApJ, 405, 538
 Carignan, C., Beaulieu, S., & Freeman, K.C. 1990, AJ, 99, 178
 Colpi, M., Mayer, L., & Governato, F. 1999, ApJ, 525, 720
 Cote, S., Freeman, K.C., & Carignan C. 1997, ASP conference series, Vol. 117, p.52
 de Blok, W.J.G., & McGaugh, S. S., 1997, MNRAS, 290, 533
 Dekel, A., & Silk, J. 1986, ApJ, 303, 39
 Dikaiakos, M., & Stadel, J. 1996, Conf. Proc. of the International Conference on Supercomputing (New York: Assoc. for Computing Machinery)
 Einasto, J., Saar, E., Kaasik, A., & Chernin, A. D. 1974, Nature, 252, 111-1
 Faber, S.M., & Lin, D.N.C. 1983, 266, ApJL, 266
 Ferguson, H.C., & Binggeli, B. 1994, AAR, 6, 6
 Ghigna, S., Moore, B., Governato, F., Lake, G., Quinn, T., Stadel J. 1998, MNRAS, 300, 146
 Gilmore, G.F. et al. 1998, Proc. SPIE, 3350, 541
 Grebel, E.K. 1999 IAU Symp. 192, Cape Town, in press, eds. White-lock, P. & Cannon (Gr99)
 Guzmán, R. et al. 1997, ApJ, 489, 559
 Helmi, A., White, S.D.M., de Zeeuw, P., & Zhao, H. 1999, Nature, 402, 53
 Hernandez, X., Gilmore, G., & Valls-Gabaud, David. 2000, to appear in MNRAS (astro-ph/0001337)
 Hernquist, L. 1993, ApJS, 86, 289
 Hoffman, G.L., Salpeter, E.E., Farhat, B., Roos, T., Williams, H. & Helou, G., 1996, ApJ, 105, 269
 Irwin, M., & Hatzidimitriou, D. 1995, MNRAS, 277, 1354
 Jobin, M., & Carignan, C. 1990, AJ, 100, 648
 Kennicutt, R.C.Jr. 1998, ApJ, 498, 541
 Klypin, A., Kravtsov, A.V., Valenzuela, O., & Prada, F. 1999, ApJ, 522, 8
 Kormendy, J. 1985, ApJ, 295, 73
 Lacey, C., & Cole, S. 1993, MNRAS, 262, 627
 Lake, G., 1990, MNRAS, 244, 701
 Little, B., & Tremaine, S. 1987, ApJ, 320, 493
 Majewski, S.R., Ostheimer, J.C., Patterson, R.J., Kunkel, W.E., Johnston, K.V., & Geisler, D. 2000, AJ, 119, 760
 Mateo, M. 1998, ARAA, 36, 435 (Ma98)
 Mo, H.J., Mao, S., & White, S.D.M. 1998, MNRAS, 296, 847
 Moore, B., Katz, N., Lake, G., Dressler, A., & Oemler, A.Jr. 1996, Nature, 379, 613
 Moore, B., Lake, G., & Katz, N. 1998, ApJ, 495, 139
 Moore, B., Ghigna, S., Governato, F., Lake, G., Quinn, T., Stadel, J., & Tozzi, P. 1999, ApJL, 524, L19-L22
 Murali, C. 2000, ApJL, 529, L81
 Peebles, P.J.E., Melott, A.L., Holmes, M.R., & Jiang, L.R. 1989, ApJ, 345, 1989
 Raha, N., Sellwood, J.A., James, R.A., & Kahn, F.D. 1991, Nature, 352, 411
 Van den Bergh, S. 1996, PASP, 108, 986
 Van den Bergh, S. 1999, AAR, 9, 273
 Wadsley, J., Quinn, T., & Stadel, J. in preparation
 Wilkinson, M.I., & Evans, N.W. 1999, MNRAS, 310, 645
 Zwaan, M. A., van der Hulst, J.M., de Blok, W.J.G., & McGaugh, S. S. 1995, MNRAS, 273, L35